Thermal Spreading Resistance in Ballistic-Diffusive Regime for GaN HEMTs

Yu-Chao Hua, Han-Ling Li, and Bing-Yang Cao

***Abstract*— To develop an efficient thermal design for gallium-nitride (GaN) high-electron-mobility transistors (HEMTs) that usually hold a super-high-power density, it is essential to accurately predict the junction temperature. In GaN HEMTs, the heat transfer process is dominated by thermal spreading resistance. Moreover, the phonon mean free paths (MFPs) of GaN are comparable with the channel layer thickness and the heat spot width. Thus, a ballistic effect emerges, resulting in the invalidity of Fourier's heat conduction law. Therefore, Fourier's law-based thermal resistance model should be reexamined and modified for this case. In this paper, we used the phonon Monte Carlo (MC) method to investigate the thermal spreading resistance in a ballistic-diffusive regime for GaN HEMTs. Our simulation results indicate that the ballistic effect significantly altered the temperature distributions within channel layers and resulted in a dramatic increase in the thermal resistance when compared with Fourier's law-based predictions. Furthermore, a semiempirical thermal resistance model with a fitting parameter was derived. This model can accurately address the issues of thermal spreading and the ballistic effect. This paper can provide a more in-depth understanding of the thermal spreading resistance in a ballistic-diffusive regime, and it can be useful for the prediction of junction temperatures and for the thermal management of HEMTs.**

***Index Terms*— Ballistic transport, high-electron-mobility transistor (HEMT), phonon Monte Carlo (MC) simulation, thermal spreading resistance.**

I. Introduction

GALLIUM-NITRIDE (GaN) high-electron-mobility transistors (HEMTs) are essential and important devices for high-frequency power amplifier and switching applications [1], [2]. Owing to their super-high-power density, GaN HEMTs hold very high junction temperature, resulting in serious thermal reliability concerns [3]–[9]. The typical structure of GaN HEMTs [7], [10] is shown in Fig. 1. The basic form of this structure is made of multilayer films. The thickness of the thinnest layer is less than 10 nm, whereas the thickness of the thickest layer (substrate) can reach about 100 μm. A large amount of heat is generated on the top surface of the GaN channel layer, the thickness of which usually ranges from 1 to 3 μm. It should be noted that the width of the heat generation area is approximately 100 nm. In other words, HEMTs hold a very small heat source area compared with the channel layer length and width [11]. When the heat spreads from a small area to a much larger substrate, there is a significant near-junction thermal resistance, or thermal spreading resistance [12], that can dominate the heat transfer process within HEMTs. The high-power density and the small heating area lead to a dramatic temperature increase during the device operation period. It is important to accurately predict the junction temperature and to reduce the device temperature through innovative thermal designs for the further development of GaN HEMTs [7], [10].

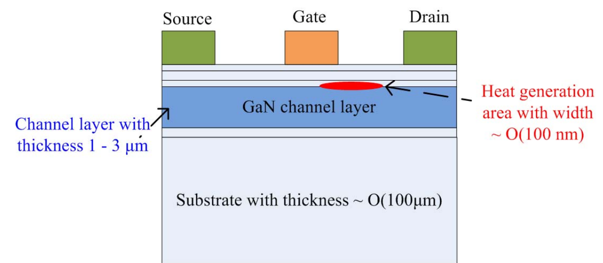

Fig. 1. Typical structure of GaN HEMTs.

Thermal spreading resistance has been extensively studied. The great majority of the existing models and simulations are based on Fourier's heat conduction law. Muzychka *et al.* [12] derived a general solution for the thermal spreading resistance for eccentric heat sources on rectangular plates. Then, Muzychka *et al.* [6] and Gholami and Bahrami [13] extended Fourier's law-based model to cases involving interfacial resistance, anisotropy, and arbitrarily located hot spots. In addition, based on Fourier's law, Darwish *et al.* [5] developed an HEMT thermal resistance model in a more practical case and improved the model by considering the temperature dependence of thermal conductivity [14].

Manuscript received April 1, 2019; revised May 22, 2019; accepted May 30, 2019. Date of publication July 8, 2019; date of current version July 23, 2019. This work was supported in part by the National Natural Science Foundation of China under Grant 51825601 and Grant 51676108, in part by the Initiative Postdocs Supporting Program of China Postdoctoral Science Foundation under Grant BX20180155, in part by the Project by the China Postdoctoral Science Foundation under Grant 2018M641348, in part by the Science Fund for Creative Research Group under Grant 51321002, and in part by the Tsinghua National Laboratory for Information Science and Technology of China (TNList). The review of this paper was arranged by Editor J. Mateos. *(Corresponding author: Bing-Yang Cao.)*

The authors are with the Department of Engineering Mechanics, Tsinghua University, Beijing 100084, China (e-mail: huayuchao19@163.com; li-hl16@mails.tsinghua.edu.cn; caoby@tsinghua.edu.cn).

Color versions of one or more of the figures in this paper are available online at http://ieeexplore.ieee.org.

Digital Object Identifier 10.1109/TED.2019.2922221

0018-9383 © 2019 IEEE. Personal use is permitted, but republication/redistribution requires IEEE permission.
See http://www.ieee.org/publications_standards/publications/rights/index.html for more information.

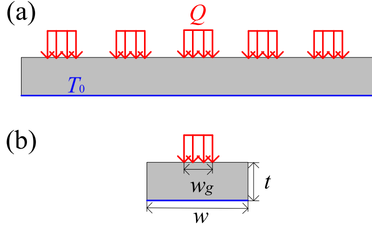

Fig. 2. Schematic for the basic system under consideration with (a) multiple periodically arrayed heat spots and (b) a single period.

The dominant heat carriers in semiconductors are phonons whose mean free paths (MFPs) are generally larger than 100 nm [15]–[18]. For GaN in particular, the frequency-domain thermoreflectance (FDTR) experiments by Ziade *et al.* [16] identified a strong size dependence of the film thermal conductivity with thickness ranging from 10 to 1000 nm in the temperature range of 300 K $< T <$ 600 K. Using the Monte Carlo (MC) method, Ma *et al.* [19] found that size effect should be considered as a GaN sample's characteristic dimension is less than 10 μm. Freedman *et al.* [18] found that phonons with MFPs larger than 1000 nm $\pm$ 200 nm contribute to 50% of GaN thermal conductivity near room temperature. Specifically, the phonon MFPs of GaN are comparable with the channel layer thickness and the heat generation width of HEMTs. In this case, Fourier's law becomes inapplicable, and the ballistic-diffusive heat conduction emerges [20]–[23] with the significant influence of ballistic transport and phonon boundary scattering that can affect the junction temperature. This necessitates the reexamination and clarification of Fourier's law-based models for spreading thermal resistance.

In this paper, the thermal spreading resistance in a ballistic-diffusive regime was studied by phonon MC simulations. Then, Fourier's law-based thermal spreading resistance model was reexamined. It was found that the ballistic effect could significantly alter the temperature distributions within channel layers and greatly increase the thermal resistance. With regard to this, we improved the thermal spreading resistance model to consider the ballistic effect. This improvement could be helpful for the junction temperature prediction and thermal management of GaN HEMTs and HEMT-like devices.

II. Problem Formulation and Simulation Details

Fig. 2(a) shows a basic system with multiple periodically arrayed heat spots. This system is a representative 2-D simplified model for the thermal spreading resistance of the GaN channel layer in HEMTs. As shown in Fig. 2(b), the thickness of the structure is t and the width of a single period is w. The heating power for each period is denoted by Q, with the heating area width equal to w_g. In general, $w_g \ll w$ in HEMTs and the MFPs of GaN are comparable with both t and w_g. In this paper, ballistic-diffusive heat conduction was simulated using the phonon MC method. This technique has proven to be a favorable stochastic method for solving the phonon Boltzmann transport equation (BTE) [20], [22]. It can deal well with the transport problems involving complicated geometries, multiple scattering events, and even the heat wave effect. The basic principles and procedures of phonon MC simulation can be found in [24] and [25]. In this research problem, the gray-media approximation [26], [27] was adopted for simplicity, and thus, all the parameters could be converted into being dimensionless. This measure could thus avoid the errors resulting from the choice of a GaN phonon MFP and facilitate the model derivation by analyzing the simulation results. Then, phonon dispersion could be incorporated using integral over phonon modes [28]–[30]. In phonon MC simulations, phonons originate from the top surface of a heating area. The boundaries in the lateral direction are set as periodic, whereas the bottom boundary serves as an absorbing boundary. The errors of the MC simulations decrease with the increasing sampling number. In this paper, the sampling number was set as 1e7, which corresponded to negligible uncertainties and guaranteed the convergence after verification. For comparison, the finite-element method (FEM) was used to simulate the diffusive heat conduction within the same system based on Fourier's law.

Both the phonon MC and FEM simulations calculated the average temperature rise of the heat generation area, and the total thermal resistance was defined as [12]

$$R = \frac{\int_{\text{heating area}} \Delta T dS}{Q} = R_{\text{sp}} + R_{\text{1-D}} \tag{1}$$

where R_{sp} is the spreading thermal resistance and $R_{\text{1-D}}$ is the 1-D thermal resistance. For the case of purely diffusive heat conduction, the 1-D thermal resistance is defined using the intrinsic thermal conductivity, κ_0, that is, $R_{\text{1-D_0}} = t/(w\kappa_0)$. In contrast, the channel layer effective thermal conductivity, $\kappa_{\text{eff_}t}$, involving the ballistic effect in the cross-plane direction should be applied to calculate the 1-D thermal resistance in a ballistic-diffusive regime [31], [32], i.e., $R_{\text{1-D_}t} = t/(w\kappa_{\text{eff_}t})$.

III. Results and Discussion

A. Thermal Resistance in the Ballistic-Diffusive Regime

A dimensionless total thermal resistance was introduced

$$\frac{R}{R_{\text{1-D_0}}} = 1 + \frac{R_{\text{sp}}}{R_{\text{1-D_0}}}. \tag{2}$$

Clearly, the analyses of the dimensionless total thermal resistance and the dimensionless thermal spreading resistance should be equivalent. This section focuses on analyzing the dimensionless total thermal resistance, since we found that it was easier to identify a phenomenological prediction model. Two Knudsen numbers [26], Kn_t and Kn_w, were defined to characterize the strength of the ballistic effect, $\text{Kn}_t = l_0/t$, and $\text{Kn}_w = l_0/w_g$, where l_0 is the intrinsic phonon MFP.

Fig. 3 shows the dimensionless temperature distributions predicted by the FEM and MC simulations. The dimensionless temperature, θ, was defined as $\theta = \Delta T/(\text{QR}_{\text{1-D_0}})$. The dimensionless temperature profiles calculated by FEM indicate the thermal spreading effect alone led to the significant increase in the peak value of dimensionless temperature. When $w/t = 40$ and $w_g/w = 0.01$, the peak value reached about 25-fold of that in 1-D heat conduction process. In addition, as indicated by the MC simulations, ballistic effect changed the configuration of the dimensionless temperature profiles

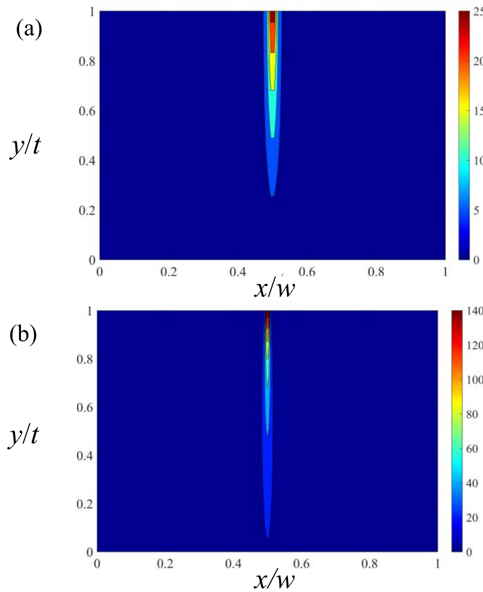

Fig. 3. Dimensionless temperature distributions with $w/t = 40$ and $w_g/w = 0.01$, predicted by FEM and MC simulations. (a) FEM. (b) MC, $Kn_t = 2$, and $Kn_w = 5$.

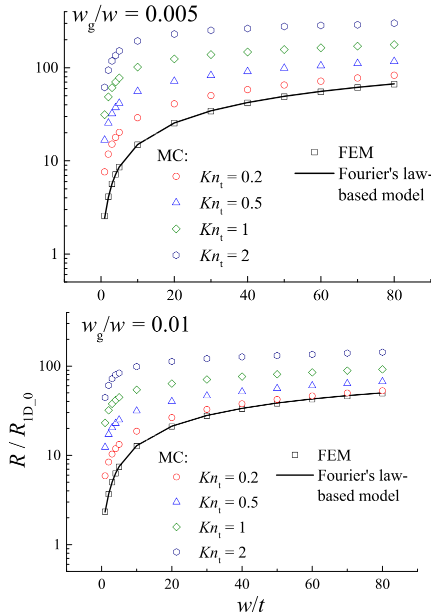

Fig. 4. Dimensionless total thermal resistance as a function of w/t, with $w_g/w = 0.005$ and 0.01.

and further increased the peak value of the dimensionless temperature. The ballistic transport caused the lack of internal phonon scatterings and caused the hot areas predicted by the MC simulation to be longer and narrower. Similarly, the MC simulation with $\mathrm{Kn}_t = 2$ and $\mathrm{Kn}_w = 5$ predicted that the peak value of the dimensionless temperature would reach about 140. The changes in the dimensionless temperature profiles resulted in a significant increase in the thermal resistance when compared with Fourier's law-based prediction.

Fig. 4 compares the values of the dimensionless total thermal resistance calculated by the phonon MC method, FEM, and Fourier's law-based model. For the structure shown in Fig. 2, according to [12], an analytical model of the total thermal resistance can be derived based on Fourier's law

$$\frac{R_F}{R_{\text{1-D_0}}} = 1 + \frac{w/t}{(w_g/w)^2} \sum_{n=1}^{\infty} \frac{\sin^2[(w_g/w)n\pi]}{n\pi} \frac{e^{[4n\pi(t/w)]} - 1}{e^{[4n\pi(t/w)]} + 1}. \tag{3}$$

As shown in Fig. 4, when considering only the thermal spreading effect, the dimensionless thermal resistance is dependent on w_g/w and w/t. The dimensionless thermal resistance increased with the decreasing w_g/w, that is, the enhancement of the thermal spreading effect. In addition, the dimensionless thermal resistance increased and approached a plateau value, w_g/w, with the increasing w/t. We noted that the FEM results agreed with the model's predictions, indicating that the model addresses the thermal spreading effect well for the thermal resistance. Furthermore, our MC simulations showed that the w_g/w- and w/t-dependent behavior of the dimensionless thermal resistance stayed almost the same in the ballistic-diffusive regime as the behavior predicted by Fourier's law-based model and simulations. In fact, the ballistic effect was dominant near the boundaries, and the diffusive transport picture could still be valid for the domains away from the boundaries. Therefore, we deduced that the expression derived from Fourier's law could be used to approximately characterize the thermal spreading effect, even in the ballistic-diffusive regime.

The values of dimensionless total thermal resistance significantly increase in the ballistic-diffusive regime when compared with those in the purely diffusive regime. As shown in Fig. 4, with the Knudsen number, Kn_t, increasing from 0.2 to 2, ballistic effect was enhanced, leading to the increase in total thermal resistance [25], [27], [33]. Kn_w, is not shown in Fig. 4, since it is not independent

$$Kn_w = Kn_t/[(w_g/w)(w/t)]. \tag{4}$$

In order to clarify the Kn_w dependence, a thermal resistance ratio was introduced, $r = R_{\mathrm{MC}}/R_F$, where R_{MC} is the total thermal resistance calculated by MC simulations and R_F is the total thermal resistance predicted by Fourier's law. The thermal spreading effect relevant to the geometrical parameters w_g/w and w/t was canceled in this thermal resistance ratio, and thus, this ratio could reflect the ballistic effect on the thermal resistance.

Fig. 5 shows the thermal resistance ratio varying with the Knudsen numbers. The independent geometrical parameter, w_g/w, is not illustrated. It was found that the thermal resistance ratio was larger than 1 and it increased with the increasing Kn_w. This means that ballistic effect emerged when the heat spot width was comparable with the MFP, and it significantly enhanced the total thermal resistance when compared with that predicted by Fourier's law. Several researchers have investigated this effect [34], [35], and the thermal gating method for thermal conductivity measurements is based on this effect [36], [37]. Furthermore, referring to the subfigures in Fig. 5, the Kn_w-dependent behavior of the thermal resistance ratio could be affected by the values of the geometrical parameters. For instance, in the case of $w/t = 80$,

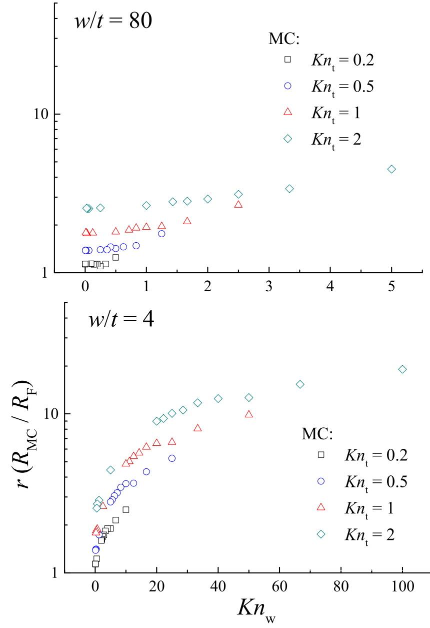

Fig. 5. Thermal resistance ratio as a function of Kn_w, with $w/t = 80$ and 4.

the curves were nearly convex, whereas they became different as $w/t = 4$. We noted that although the curves of $w/t = 4$ became different, the thermal resistance ratio still increased with the increasing Kn_w, and it did not approach a plateau.

B. Model Derivation for the Thermal Resistance in the Ballistic-Diffusive Regime

The key issue here was finding an applicable thermal resistance model that involved the ballistic effect for HEMTs and HEMT-like devices. First, we could model the channel layer effective thermal conductivity, κ_{eff_t}, involving the ballistic effect in the cross-plane direction with the differential approximation and the temperature jump boundary conditions [26], and thus, we had

$$\frac{\partial^2 T}{\partial x^2} = 0; \quad \left\{ Q = -\kappa_0 w \left.\frac{\partial T}{\partial x}\right|_0, \quad T|_t - T_0 = -\frac{2}{3} l_0 \left.\frac{\partial T}{\partial x}\right|_t \right\}. \tag{5}$$

Solving the above equations yielded the formula to predict the 1-D thermal resistance involving the cross-plane ballistic effect

$$R_{\text{1-D_}t} = R_{\text{1-D_0}} \left(1 + \frac{2}{3} Kn_t\right). \tag{6}$$

Fig. 6 shows that the ratio between R_{1-D_t} and R_{1-D_0} linearly increased with the increasing Kn_t. When comparing our model's predictions to the MC simulation results, good agreements were achieved, with the maximum deviation less than 10%.

We rearranged the formula of thermal resistance to

$$\frac{R_{\text{MC}}}{R_{\text{1-D_0}}} = \frac{R_F}{R_{\text{1-D_0}}} \frac{R_{\text{1-D_}t}}{R_{\text{1-D_0}}} \left[\frac{R_{\text{MC}}}{R_{\text{1-D_t}}} \left(\frac{R_F}{R_{\text{1-D_0}}} \right)^{-1} \right] \tag{7}$$

where the analytical expressions for $R_F / R_{\text{1-D_0}}$ and $R_{\text{1-D_}t} / R_{\text{1-D_0}}$ have been obtained from (3) and (6). The first term, $R_F / R_{\text{1-D_0}}$, describes the thermal spreading effect, whereas the second term, $R_{\text{1-D_}t} / R_{\text{1-D_0}}$, represents the cross-plane ballistic effect.

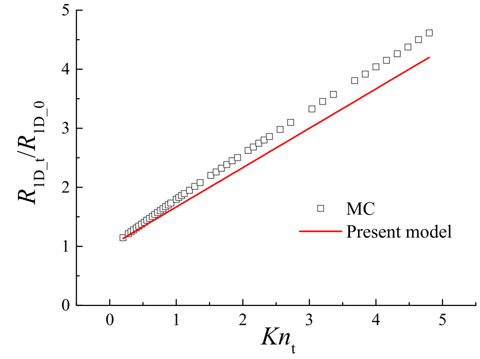

Fig. 6. Ratio between the 1-D thermal resistance in the ballistic-diffusive regime and that calculated by Fourier's law.

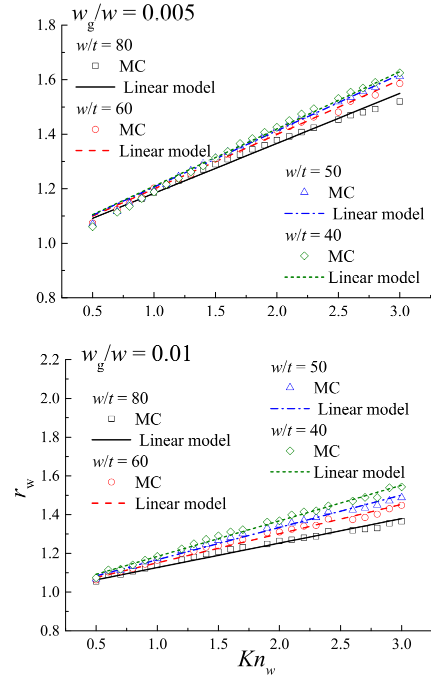

Fig. 7. Ratio, r_w, as a function of Kn_w, with $w_g/w = 0.005$ and 0.01.

Therefore, the third term denoted by r_w

$$r_w = \frac{R_{\text{MC}}}{R_{\text{1-D_t}}} \left(\frac{R_F}{R_{\text{1-D_0}}} \right)^{-1} \tag{8}$$

was supposed to reflect the ballistic effect with w_g comparable with MFP. Fig. 7 shows that r_w increased almost linearly with Kn_w increasing. Therefore, we proposed a linear function to approximately characterize $r_w = 1 + A_w Kn_w$, with a fitting parameter A_w. The intercept of the above linear function is supposed to be unity, since r_w should approach unity in the limiting case of $Kn_w = 0$. Moreover, the fitting parameter, A_w, should depend on the geometrical parameters, w_g/w and w/t. The corresponding dependent behavior is shown in Fig. 8. It was found that A_w decreased with the increasing w/t and w_g/w in the given ranges. The ballistic effect was

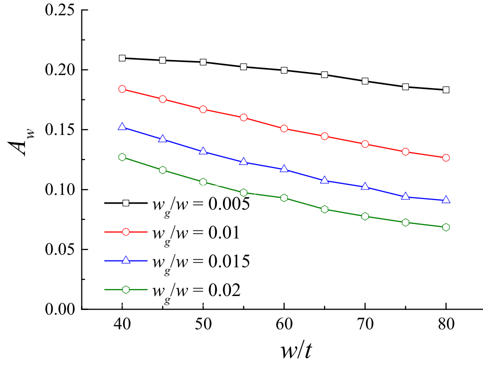

Fig. 8. Fitting parameter A_W varying with w_g/w and w/t.

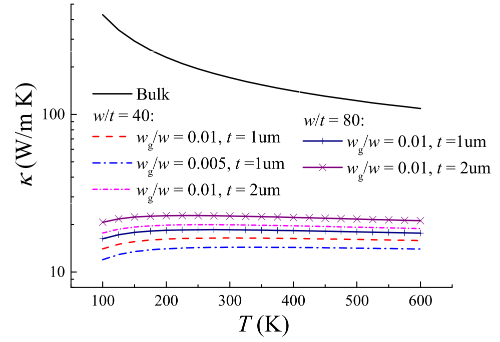

Fig. 9. Effective thermal conductivity as a function of temperature, with comparison to the bulk value.

significantly affected by the dimensions and geometries of nanostructures [23], which is shown in Fig. 8. The dependence of the thermal resistance ratio on w/t and w_g/w can be attributed to this point.

We obtained a semiempirical prediction model for the thermal resistance involving the effects of thermal spreading and ballistic transport

$$\frac{R}{R_{\text{1-D_0}}} = \frac{R_F}{R_{\text{1-D_0}}}\left(1+\frac{2}{3}Kn_t\right)(1+A_w Kn_w) \tag{9}$$

in which R_{1-D_0} could be readily calculated using intrinsic thermal conductivity. The first term characterizes the thermal spreading effect, the second term $1 + 2/3Kn_t$ corresponds to the cross-plane ballistic effect, and the third term $1+A_w Kn_w$ represents the ballistic effect that occurs because w_g is comparable with the MFP. An effective thermal conductivity could be derived from the present model, that is

$$\frac{\kappa_{\text{eff}}}{\kappa_0} = \frac{1}{(1+A_w(w_g/w, w/t)Kn_w)\left(1+\frac{2}{3}Kn_t\right)}. \tag{10}$$

Once the geometrical parameters and a representative phonon MFP were given, the combination of this effective thermal conductivity model and Fourier's law-based thermal spreading model could estimate the thermal resistance in a ballistic-diffusive regime. Although our model was derived with the gray-media approximation (i.e., single phonon mode), it was easy to extend the model to the case involving phonon dispersions with an integral over the phonon modes [28]

$$\kappa_{\text{eff}} = \frac{1}{3}\sum_j \int_0^{\omega_j} \hbar\omega \frac{\partial f_0}{\partial T} v_{g\omega j} l_{j,m} \text{DOS}_j(\omega) d\omega \tag{11}$$

with the modified MFPs

$$l_{m,j} = \frac{l_{0,j}}{(1+A_w(w_g/w, w/t)Kn_{w_\omega,j})\left(1+\frac{2}{3}Kn_{t_\omega,j}\right)} \tag{12}$$

where $l_{0,j}$ is the intrinsic frequency-dependent MFP of the j branch phonon and $Kn_{w_\omega,j} = l_{0,j}/w_g$ and $Kn_{t_\omega,j} = l_{0,j}/t$ are the frequency-dependent and phonon branch-dependent Knudsen numbers. Following the methodology described previously, we could calculate the effective thermal conductivity applicable for the GaN channel layers with narrow heating areas. For bulk GaN, Morelli *et al.* [38] proposed an improved Debye–Callaway model that considered the frequency dependence and temperature dependence of phonon scattering to calculate the GaN's intrinsic thermal conductivity. Equation (12) could be applied to modify the model by Morelli *et al.* [38] to estimate the effective thermal conductivity of GaN channel layers. We suggest that the gray model may be used as a simplification in the case where the temperature difference is small. By contrast, when the temperature effect is significant, the improved model should be more applicable.

As shown in Fig. 9, the significant reduction in the effective thermal conductivities when compared with the bulk values underscores the importance of the ballistic effects. This also indicates that the majority of phonons that transport heat in GaN held the rather long MFPs. The effective thermal conductivity increased with the increasing channel layer thickness due to the degradation of the cross-plane ballistic effect's strength. Because the thickness was known, the effective thermal conductivity decreased with the reduced w/t and w_g/w. Moreover, the intrinsic thermal conductivity decreased with the increasing temperature in the range of 100–600 K, whereas the effective thermal conductivity experienced a very different temperature-dependent behavior resulting from the ballistic effect. It first increased and then slightly decreased with the increasing temperature. This happened because the MFPs were dominated by the structure dimensions that did not vary with temperature, leading to the nonsignificant temperature dependence.

IV. Conclusion

In this paper, we investigated the thermal spreading resistance in a ballistic-diffusive regime specific to GaN HEMTs using FEM and the phonon MC method. It was determined that the ballistic effect significantly changed the temperature distributions within channel layers. When compared with Fourier's law-based predictions, the temperature distributions in the ballistic-diffusive regime hold narrower and longer hot areas and much larger peak values of the temperature rise, which leads to a dramatic increase in the thermal resistance and a violation of Fourier's law-based model for this case. A semi-empirical thermal resistance model that could consider the influence of both thermal spreading and the ballistic effect was derived from the combination of phonon BTE and an analysis of the simulation results. This paper provides a more in-depth

understanding of the thermal spreading process involving the ballistic effect. The model can be useful for the thermal management of GaN HEMTs and HEMT-like devices.

REFERENCES

[1] U. K. Mishra, P. Parikh, and Y.-F. Wu, "AlGaN/GaN HEMTs—An overview of device operation and applications," *Proc. IEEE*, vol. 90, no. 6, pp. 1022–1031, Jun. 2002. doi: 10.1109/JPROC.2002.1021567.

[2] K. Hirama, M. Kasu, and Y. Taniyasu, "RF high-power operation of AlGaN/GaN HEMTs epitaxially grown on diamond," *IEEE Electron Device Lett.*, vol. 33, no. 4, pp. 513–515, Apr. 2012. doi: 10.1109/Led.2012.2185678.

[3] Z. Liao *et al.*, "Thermal evaluation of GaN-based HEMTs with various layer sizes and structural parameters using finite-element thermal simulation," *Microelectron. Rel.*, vol. 74, pp. 52–57, Jul. 2017. doi: 10.1016/j.microrel.2017.05.012.

[4] J. W. Pomeroy, M. J. Uren, B. Lambert, and M. Kuball, "Operating channel temperature in GaN HEMTs: DC versus RF accelerated life testing," *Microelectron. Rel.*, vol. 55, pp. 2505–2510, Dec. 2015. doi: 10.1016/j.microrel.2015.09.025.

[5] A. M. Darwish, A. J. Bayba, and H. A. Hung, "Thermal resistance calculation of AlGaN-GaN devices," *IEEE Trans. Microw. Theory Techn.*, vol. 52, no. 11, pp. 2611–2620, Nov. 2004. doi: 10.1109/tmtt.2004.837200.

[6] Y. S. Muzychka, K. R. Bagnall, and E. N. Wang, "Thermal spreading resistance and heat source temperature in compound orthotropic systems with interfacial resistance," *IEEE Trans. Compon., Packag., Manuf. Technol.*, vol. 3, no. 11, pp. 1826–1841, Nov. 2013. doi: 10.1109/Tcpmt.2013.2269273.

[7] A. Stocco, "Reliability and failure mechanisms of GaN HEMT devices suitable for high-frequency and high-power applications," Ph.D. dissertation, Dept. Inf. Eng., Univ. Padova, Padova, Italy, 2012.

[8] Y. Won, J. Cho, D. Agonafer, M. Asheghi, and K. E. Goodson, "Cooling limits for GaN HEMT technology," in *Proc. IEEE Compound Semiconductor Integr. Circuit Symp. (CSICS)*, Monterey, CA, USA, Oct. 2013, pp. 1–5. doi: 10.1109/CSICS.2013.6659222.

[9] J. Cho, Y. Li, W. E. Hoke, D. H. Altman, M. Asheghi, and K. E. Goodson, "Phonon scattering in strained transition layers for GaN heteroepitaxy," *Phys. Rev. B, Condens. Matter*, vol. 89, no. 12, pp. 115301-1–115301-11, Mar. 2014. doi: 10.1103/PhysRevB.89.115301.

[10] Y. Won, J. Cho, D. Agonafer, M. Asheghi, and K. E. Goodson, "Fundamental cooling limits for high power density gallium nitride electronics," *IEEE Trans. Compon., Packag., Manuf. Technol.*, vol. 5, no. 6, pp. 737–744, Jun. 2015. doi: 10.1109/TCPMT.2015.2433132.

[11] A. Sarua *et al.*, "Thermal boundary resistance between GaN and substrate in AlGaN/GaN electronic devices," *IEEE Trans. Electron Devices*, vol. 54, no. 12, pp. 3152–3158, Dec. 2007. doi: 10.1109/TED.2007.908874.

[12] Y. S. Muzychka, J. R. Culham, and M. M. Yovanovich, "Thermal spreading resistance of eccentric heat sources on rectangular flux channels," *J. Electron. Packag.*, vol. 125, no. 2, pp. 178–185, 2003. doi: 10.1115/1.1568125.

[13] A. Gholami and M. Bahrami, "Thermal spreading resistance inside anisotropic plates with arbitrarily located hotspots," *J. Thermophys. Heat Transf.*, vol. 28, no. 4, pp. 679–686, Aug. 2014. doi: 10.2514/1.T4428.

[14] A. Darwish, A. J. Bayba, and H. A. Hung, "Channel temperature analysis of GaN HEMTs with nonlinear thermal conductivity," *IEEE Trans. Electron Devices*, vol. 62, no. 3, pp. 840–846, Mar. 2015. doi: 10.1109/Ted.2015.2396035.

[15] B. A. Danilchenko, T. Paszkiewicz, S. Wolski, A. Jeżowski, and T. Plackowski, "Heat capacity and phonon mean free path of wurtzite GaN," *Appl. Phys. Lett.*, vol. 89, no. 6, Aug. 2006, Art. no. 061901. doi: 10.1063/1.2335373.

[16] E. Ziade, J. Yang, G. Brummer, D. Nothern, T. Moustakas, and A. J. Schmidt, "Thickness dependent thermal conductivity of gallium nitride," *Appl. Phys. Lett.*, vol. 110, no. 3, Jan. 2017, Art. no. 031903. doi: 10.1063/1.4974321.

[17] L. Lindsay, D. A. Broido, and T. L. Reinecke, "Thermal conductivity and large isotope effect in GaN from first principles," *Phys. Rev. Lett.*, vol. 109, Aug. 2012, Art. no. 095901. doi: 10.1103/PhysRevLett.109.095901.

[18] J. P. Freedman, J. H. Leach, E. A. Preble, Z. Sitar, R. F. Davis, and J. A. Malen, "Universal phonon mean free path spectra in crystalline semiconductors at high temperature," *Sci. Rep.*, vol. 3, p. 2963, Oct. 2013. doi: 10.1038/srep02963.

[19] J. Ma, X. Wang, B. Huang, and X. Luo, "Effects of point defects and dislocations on spectral phonon transport properties of wurtzite GaN," *J. Appl. Phys.*, vol. 114, Aug. 2013, Art. no. 074311. doi: 10.1063/1.4817083.

[20] H. Bao, J. Chen, X. Gu, and B.-Y. Cao, "A review of simulation methods in micro/nanoscale heat conduction," *ES Energy Environ.*, vol. 1, pp. 16–55, Sep. 2018. doi: 10.30919/esee8c149.

[21] Z.-Y. Guo, "Energy-mass duality of heat and its applications," *ES Energy Environ.*, vol. 1, pp. 4–15, Sep. 2018. doi: 10.30919esee8c146.

[22] D. G. Cahill *et al.*, "Nanoscale thermal transport. II. 2003–2012," *Appl. Phys. Rev.*, vol. 1, Jan. 2014, Art. no. 011305. doi: 10.1063/1.4832615.

[23] Y.-C. Hua and B.-Y. Cao, "Ballistic-diffusive heat conduction in multiply-constrained nanostructures," *Int. J. Therm. Sci.*, vol. 101, pp. 126–132, Mar. 2016. doi: 10.1016/j.ijthermalsci.2015.10.037.

[24] Y.-C. Hua and B.-Y. Cao, "An efficient two-step Monte Carlo method for heat conduction in nanostructures," *J. Comput. Phys.*, vol. 342, pp. 253–266, Apr. 2017. doi: 10.1016/j.jcp.2017.04.042.

[25] Y.-C. Hua and B.-Y. Cao, "Phonon ballistic-diffusive heat conduction in silicon nanofilms by Monte Carlo simulations," *Int. J. Heat Mass Transf.*, vol. 78, pp. 755–759, Nov. 2014. doi: 10.1016/j.ijheatmasstransfer.2014.07.037.

[26] Y.-C. Hua and B.-Y. Cao, "Slip boundary conditions in ballistic-diffusive heat transport in nanostructures," *Nanosc. Microscale Thermophys. Eng.*, vol. 21, pp. 159–176, Jul. 2017. doi: 10.1080/15567265.2017.1344752.

[27] A. Majumdar, "Microscale heat conduction in dielectric thin films," *J. Heat Transf.*, vol. 115, no. 1, pp. 7–16, Feb. 1993. doi: 10.1115/1.2910673.

[28] N. Mingo, "Calculation of Si nanowire thermal conductivity using complete phonon dispersion relations," *Phys. Rev. B, Condens. Matter*, vol. 68, Sep. 2003, Art. no. 113308. doi: 10.1103/PhysRevB.68.113308.

[29] Y.-C. Hua and B.-Y. Cao, "Cross-plane heat conduction in nanoporous silicon thin films by phonon Boltzmann transport equation and Monte Carlo simulations," *Appl. Therm. Eng.*, vol. 111, pp. 1401–1408, Jan. 2017. doi: 10.1016/j.applthermaleng.2016.05.157.

[30] M. Ohnishi and J. Shiomi, "Towards ultimate impedance of phonon transport by nanostructure interface," *APL Mater.*, vol. 7, Jan. 2019, Art. no. 013102. doi: 10.1063/1.5055570.

[31] Y.-C. Hua and B.-Y. Cao, "The effective thermal conductivity of ballistic-diffusive heat conduction in nanostructures with internal heat source," *Int. J. Heat Mass Transf.*, vol. 92, pp. 995–1003, Jan. 2016. doi: 10.1016/j.ijheatmasstransfer.2015.09.068.

[32] J. Kaiser, T. Feng, J. Maassen, X. Wang, X. Ruan, and M. Lundstrom, "Thermal transport at the nanoscale: A Fourier's law vs. phonon Boltzmann equation study," *J. Appl. Phys.*, vol. 121, Jan. 2017, Art. no. 044302. doi: 10.1063/1.4974872.

[33] D. P. Sellan, J. E. Turney, A. J. H. McGaughey, and C. H. Amon, "Cross-plane phonon transport in thin films," *J. Appl. Phys.*, vol. 108, Dec. 2010, Art. no. 113524. doi: 10.1063/1.3517158.

[34] A. A. Maznev, J. A. Johnson, and K. A. Nelson, "Onset of non-diffusive phonon transport in transient thermal grating decay," *Phys. Rev. B, Condens. Matter*, vol. 84, Nov. 2011, Art. no. 195206. doi: 10.1103/PhysRevB.84.195206.

[35] A. J. Minnich, "Determining phonon mean free paths from observations of quasiballistic thermal transport," *Phys. Rev. Lett.*, vol. 109, Nov. 2012, Art. no. 205901. doi: 10.1103/PhysRevLett.109.205901.

[36] J. A. Johnson *et al.*, "Direct measurement of room-temperature nondiffusive thermal transport over micron distances in a silicon membrane," *Phys. Rev. Lett.*, vol. 110, Jan. 2013, Art. no. 025901. doi: 10.1103/PhysRevLett.110.025901.

[37] Y. Hu, L. Zeng, A. J. Minnich, M. S. Dresselhaus, and G. Chen, "Spectral mapping of thermal conductivity through nanoscale ballistic transport," *Nature Nanotechnol.*, vol. 10, pp. 701–706, Jun. 2015. doi: 10.1038/nnano.2015.109.

[38] D. T. Morelli, J. P. Heremans, and G. A. Slack, "Estimation of the isotope effect on the lattice thermal conductivity of group IV and group III-V semiconductors," *Phys. Rev. B, Condens. Matter*, vol. 66, Nov. 2002, Art. no. 195304. doi: 10.1103/PhysRevB.66.195304.